Optimal Capacity Sizing for Completely Green Charging Systems for Electric Vehicles

Juliette Ugirumurera, Zygmunt J. Haas, *Fellow, IEEE*

Abstract—Although proliferation of electric vehicles (EVs) is associated with significant environmental benefits, these benefits would be forfeited if the associated EV charging systems would rely only on conventional power grid, whose power is mainly generated by fossil-fueled power plants. In contrast, utilizing distributed renewable energy sources (RES) will preserve and further amplify these environmental benefits. However, planning of green EV charging systems has not been adequately investigated in the technical literature. This paper studies the optimal sizing of a completely green charging system, which relies entirely on the power generated by RES, specifically by solar panels. In particular, this paper presents a methodology to determine the optimal resource size (e.g., the number of solar panels and the energy-storage capacity) that minimizes the charging system's investment costs, while meeting the charging system's performance metrics. A search-based algorithm is devised to solve the formulated nonlinear integer programming problem in order to efficiently explore the problem's solution space. A 3-D Markov chain model is used to account for the intermittency in solar power production. Finally, an example of a completely green charging system is presented to demonstrate the use of the proposed methodology.

Index Terms—Charging station model, completely green systems, electric vehicles (EVs), energy storage systems (ESSs), optimization, renewable energy sources (RES).

NOMENCLATURE

a	Coefficient of solar radiation equation.
A_k	Solar panel area size.
b	Coefficient of solar radiation equation.
B	Energy Storage state-of-charge level.
C_f	Number of kWh to fully charge EV battery.
C_s	Number of installed charging stations.
d	Charging completion probability.
D	Average delay per EV.
D_{td}	Target average delay.
e	Identity vector.
$E[V]$	Expected number of EVs.
f	EV battery level index.
F	Index for maximum EV battery demand.
g	Number of fully charged EVs.

geoinv	Inverse cumulative geometric distribution.
G	Solar radiation intensity.
h	Time-of-day period index.
H	Total number of periods per day.
h_w	Time-of-day period with smallest average solar energy.
J	Number of rows/columns in the system transition matrix.
K	Number of solar panels.
K_{max}	Upper bound for number of solar panels.
K_{opt}	Optimal number of solar panels.
l	Energy storage state index.
L	Index for completely depleted energy storage state.
m	Number of EV arrivals.
N	Number of operational charging stations.
P	System transition probability.
P_{bl}	Blocking Probability.
$\overline{p_{hw}}$	Smallest average solar energy per time-of day period.
$\mathbf{Q}$	System transition matrix.
r	Solar radiation state index.
R	Completely overcast sky state.
s	Season index.
t	Index for years.
T	Total number of years in planning horizon.
U	Discount rate.
υ	Number of EVs in the system.
V	Maximum queue capacity.
W	Present worth coefficient.
x	Number of timeslots that an EV waits before departing.
Y	Charging station rate.
z	System solution index.
$\bar{\alpha}$	System throughput.
β_{ess}	Energy storage capacity.
β_{max}	Upper bound for energy storage capacity.
β_{opt}	Energy storage optimal capacity.
γ	Ratio of per-kWh energy storage cost to per kW renewable production cost.
δ_1	Difference between EV battery levels.
δ_2	Energy difference between energy storage states.
ε	Maximum energy demand use in solution space bounding.
ζ	Solar panel investment cost per kW.
η	Solar panel efficiency.
λ	EV arrival rate.
μ_e	Energy storage annual maintenance cost per kWh.
μ_k	Solar panel annual maintenance cost per kW.

θ Available power from all solar panels.

π Steady-state probability.

$\bar{\bar{\Pi}}$ Steady-state probability vector.

ρ Solar panel output power.

$\wp$ Probability value used in upper bounds calculations.

ϱ Uniformly distribute random number in interval (0, 1).

τ Duration of timeslot.

χ Elevation angle.

ψ Solar state-transition probability.

Ψ Solar state-transition matrix.

ϕ Probability of charging EVs.

ω Solar panel maximum generating capacity.

Ω Matrix of cumulative transition probabilities.

I. INTRODUCTION

RECENTLY, growing environmental concerns, combined with the advances in the field of energy storage, have contributed to the rapid development of electric vehicle (EV) technologies. Large-scale EVs deployment in the transportation sector has the potential to reduce greenhouse emissions, increase renewable energy penetration, and save fuel cost for drivers [1]. Since EVs run exclusively on their battery's electric power, an increase in availability of public EV charging stations is crucial for EV widespread usage [2]. Accordingly, there have been works that study the optimal placement and sizing of grid-connect EV charging stations [3]–[8], where the charging energy is mainly drawn from the existing power grid. However, the use of the power grid, whose power is mainly generated by fossil-fueled power plants, reduces the overall EVs benefits and can even increase the overall emission levels as compared with the fossil-fueled vehicular systems [9].

Completely green charging systems (CGCSs) are EV charging systems, in which the energy is produced entirely by renewable energy sources (RES), such as solar panels or wind turbines. CGCSs reduce carbon emissions by charging EVs exclusively by renewable energy, thus increasing the penetration of RES in the energy sector. CGCSs also have the potential to decrease EV charging costs [10]. However, the uncertainty (e.g., daily randomness in cloud coverage for solar panels) and time-dependence (e.g., seasonal variations in sun exposure) in RES's power generation is a significant challenge in the design of CGCSs. Accordingly, energy storage systems (ESSs) are important components of CGCSs, as they helps to stabilize the RES energy production [11]. Additionally, the study of CGCSs requires the utilization of stochastic models and methods to account for the unpredictability in renewable energy production [12].

This paper presents a methodology for the optimal sizing of a CGCS for EVs, where the source of charging energy is produced entirely by solar panels. A charging system located in a secluded completely green village is considered, where the green village is a small-scale power system isolated from the main power grid. The load demands of the completely green village are met entirely by the distributed RES. Isolated green villages are appropriate for remote areas, where the expansion of the existing power grid may be impossible or impractical,

such as is often the case in developing countries. They are also useful as backup power sources for local communities in case of grid failures (physical sabotage or cyber-attacks) or other power outages (grid collapse or load shedding). Finally, because of their beneficial effect on reducing the carbon footprint and, consequently, the global warming, completely green communities are expected to become more and more common in the future. Of course, the main challenge of a completely green system, in general, and a completely green charging system, in particular, is the intermittent behavior of RES; e.g., sun radiation is not present at night or may be insufficient to meet energy demand during highly clouded days. Although different RES types may exhibit some limited complementary behavior (e.g., wind may partially compensate for the lack of nocturnal solar energy generation), this typically is insufficient for a continuous operation of a completely green system. Accordingly, some form of energy storage is required in such systems to compensate for: 1) randomness in the energy generation and 2) lack of continuous energy generation in a 24-h period of some RES types. The goal of the presented methodology is to determine the optimal number of solar panels and the ESS capacity that satisfy the EVs' charging demand and performance metrics (e.g., average EV charging delay), while minimizing the system's investment costs.

The rest of this paper is organized as follows. In Section II, existing studies related to this paper are discussed. Section III presents the system model and the problem statement, while Section IV delineates the algorithm for the solution of the formulated problem. The proposed methodology is applied to an example case study in Section V. Section VI describes the data and steps needed to successfully utilize the presented methodology in practice. Finally, Section VII concludes the paper.

II. RELATED WORKS

Recently, researchers have recognized the role of EVs in increasing the utilization of renewable energy in the power grid. Nguyen *et al.* [13] proposed to coordinate the charging/discharging of EVs to handle the frequency deviation in the power grid due to renewable energy intermittency. Reference [14] describes a distributed charging algorithm to control large EVs populations to balance the intermittent renewable generation and to allow high penetration of RES in the grid. In [15], a charging control approach was presented that manages an EV fleet, so that the cumulative power consumption of an electricity distribution network, including solar generation, approximates a specified target profile. In comparison, while [13]–[15] studied the charging/discharging of EVs to improving renewable energy utilization in a power grid, this paper studies the optimal planning of a completely green charging system that is isolated from the main power grid; i.e., a system in which the EVs charging relies exclusively on RES.

The use of RES for EV charging has been considered in a number of works. For example, [16] and [17] investigated the potential of daytime solar-based charging stations located in a workplace parking garage to cover EVs power demand. In particular, in [17] simulations results showed that 48 parking lots in Frauenfeld, Switzerland, if covered with solar carports,

could meet 15%–40% of transportation energy demand. Tulpule *et al.* [10] considered a grid-connected photovoltaic-based station located in a workplace parking garage in order to maximize the use of solar power. Similarly, [18] analyzed the possibility of charging EV batteries at workplace in Netherlands using solar energy, with the aim of minimizing grid dependence and maximizing solar power use. However, the above works [10] and [16]–[18] did not focus on the optimal sizing of the RES (e.g., to minimize the EV charging system's investment/operational costs), but rather assumed fixed RES capacity that fits the available parking lot space.

Park and Kwon [19] investigated the potential of renewable electricity generation for taxi services in Daejeon, South Korea, considering solar energy, wind energy, batteries, and electric-grid connection. The cost of energy for the resulting renewable generation system was assessed, however, without consideration of randomness in renewable energy production or EV charging performance level. In contrast, in this paper, a queueing model is utilized to formulate the charging system sizing problem in order to account for randomness and fluctuations in renewable energy generation. In particular, a multidimensional discrete-time Markov chain model is utilized, in which each system state is defined by the number of EVs, the solar radiation intensity (for solar panels' energy generation), and the ESS *state of charge (SOC)*. Additionally, unlike [19] that considered static daily EV load, the utilized queueing model allows to account for the randomness in EV arrivals, while the queueing performance measures are used to evaluate the charging system's operation. Examples of the performance measures include the system's throughput, which determines the number of EVs charged per unit time, and the expected system delay, which corresponds to the average time that an EV spends in the charging system.

III. SYSTEM MODEL

As illustrated in Fig. 1, the CGCS is a collection of EV charging stations utilizing the energy produced by solar panels and the energy discharged from the ESS. For simplicity, the system's charging stations are assumed to be identical and deliver power at the same charging rate of Y [in kilowatt (kW)]. It is also assumed that the charging system's energy is supplied by identical solar panels with the same power generation capacity (in kW).

Additionally, the following energy consumption policy is assumed for the charging system: 1) by default, EVs are charged by the power generated by the solar panels; 2) when the produced solar energy is greater than the energy necessary to operate the required number of charging stations to serve the EVs currently present in the CGCS, the excess energy is stored in the ESS; and 3) in case when the solar panels' energy is insufficient, the charging system discharges from the ESS as much energy as is available to cover the extra load. As this policy gives priority to utilizing the energy produced by solar panels, it can be derived that investment in solar power capacity will be generally larger than the investment in the energy storage capacity. This will be shown in the numerical results presented in Section V. Other energy utilization policies could be used; e.g., when the ESS is not completely
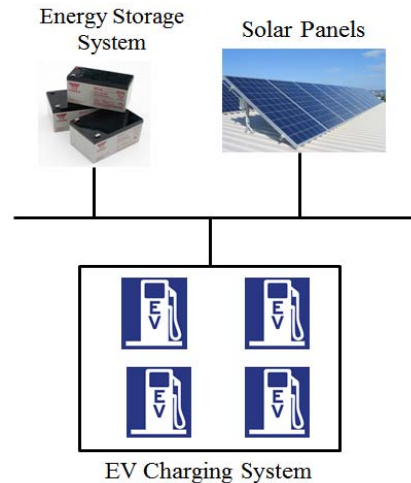

Fig. 1. Completely green EV charging system.

charged, the energy management protocol could always draw some fraction of the generated power to charge the ESS. Alternatively, the energy management protocol could put a limit on the amount of energy discharged from ESS within particular time periods. In this case, the investment in energy storage capacity would be dictated by the ESS discharge limit, and the solar panels' capacity might be higher due to this discharge ESS limit. Yet another energy management protocol could limit the solar energy and ESS energy use depending on the perceived reward from serving the EVs demand within a particular time period. With this later scheme, the ESS and solar panel capacity would depend on the particulars of the reward model.

A. EV Model

It is assumed that the maximum capacity of an EV battery is C_F, and that an EV state is characterized by its energy in kWh, C_f, needed to fully charge its battery, where $C_0 \leq C_f \leq C_F$. It is further assumed that this EV charge demand is discretized into equal-size levels: $C_0, C_1, C_2, \ldots, C_F$, where $\delta_1 = C_i - C_{i-1}$ is defined, for $0 < i \leq F$. Accordingly, $C_0 = 0$ kWh corresponds to no energy demand—i.e., a fully charged EV battery, while C_F corresponds to the maximum energy demand per EV. The duration of a timeslot $\tau = \delta_1/Y$ is the time interval required to charge an EV battery with δ_1 kWh. The choice of the value of δ_1 depends on the desired accuracy of the system model. Since in practice the EV energy demand is continuous, in the above-discretized model, a particular demand will be approximated to the closest C_f level, thus introducing some error. Of course, the smaller δ_1 is, the smaller is this discretization error.

B. Solar Panel Model

In this paper, only solar panels are considered as RES, with plans to incorporate other types of RES (e.g., wind turbines) in the future works. K identical solar panels are modeled. Each solar panel unit has a maximum power generating capacity of ω [kW] and is also associated with a per kW investment cost of ζ [$/kW], which includes equipment purchasing and installation costs. A solar panel also has a per-kW annual

r	a_0	a_1	a_2	a	b
0	-112.6	653.2	174.0	0.73	-95.0
1	-112.6	686.5	120.9	0.72	-89.2
2	-107.3	650.2	127.1	0.72	-78.2
3	-97.8	608.3	110.6	0.72	-67.4
4	-85.1	552.0	106.3	0.72	-57.1
5	-77.1	511.5	58.5	0.70	-45.7
6	-71.2	495.4	-37.9	0.70	-33.2
7	-31.8	287.5	94.0	0.69	-16.5
8	-13.7	154.2	64.9	0.69	-4.3

maintenance cost of μ_k [$/kW] [20]. The solar output power depends on the solar radiation, which is modeled following the discrete-time Markov chain presented in [21] and [22]. This discrete Markov model relies on the local cloud coverage data, which account for the effect of climatological conditions on solar radiation intensity, including cloud type, cloud movement, cloud formation and dissipation, humidity, and atmospheric pressure.

The cloud coverage is measured in Oktas, which is an indication of how many eighth parts of the sky are covered by the clouds [23]. The level of cloudiness is then expressed as an integer between 0 and 8, where 0 is the completely clear sky state and 8 corresponds to completely overcast sky [24]. Accordingly, the solar radiation intensity, G [kW/m^2], can be in any of nine distinct states: the $r = 8$ state where the sun is completely covered by clouds, so that the solar panel does not produce any power ($G_0 = 0$ [kW/m^2]); and the $r = 0$ state which corresponds to the maximum solar radiation state, where the solar panel produces its maximum power. The solar radiation intensity is obtained from the cloud coverage and the sun's elevation angle χ, as shown in (1). In (1), r refers to the number of Oktas, and the values for the constants $b(r)$, $a(r)$ and $a_i(r)$ for $i = 0, 1, 2$ are shown in Table I [25]

$$G_r = \left[\frac{a_0(r) + a_1(r)\sin\chi + a_3(r)\sin^3\chi - b(r)}{a(r)} \right]. \quad (1)$$

A detailed discussion on the elevation angle χ and the empirically determined relationship in (1) is presented in [25].

The transition probabilities between the r states are estimated from the measured cloud coverage data intuitively as shown in (2) [22], where $\psi_{i,j}$ is the estimated transition probability from state i to state j, and q_{ij} is the number of transitions within one-hour period from the cloud coverage level i to the cloud coverage level j [22], [24]

$$\psi_{i,j} = \frac{q_{ij}}{\sum_{k=0}^{8} q_{ik}}. \quad (2)$$

The transition probability matrix $\boldsymbol{\Psi}$ is then determined as

$$\boldsymbol{\Psi} = \begin{bmatrix} \psi_{0,0} & \psi_{0,1} & \cdots & \psi_{0,R} \\ \psi_{1,0} & \psi_{1,1} & \cdots & \psi_{1,R} \\ \vdots & \vdots & \ddots & \vdots \\ \psi_{R,0} & \psi_{R,1} & \cdots & \psi_{R,R} \end{bmatrix}. \quad (3)$$

Using the radiation intensity G_r, the solar panel's output power (in units of kW) is found by

$$\rho_r = \eta \cdot A_k \cdot G_r \quad (4)$$

where η and A_k represent the solar panel's efficiency (in %) and the total area of the panel (in m^2), respectively. Of course, $\rho_r \leq \omega$.

In order to account for the seasonal and time-of-day variations in the cloud coverage, different transitions matrices should be considered, each representative of a particular time-of-day period for a season in a year [22]. As an example, a typical day in a season could be represented by three matrices, one for the morning period (8am–11am), one for mid-day (11am–2pm), and another for the afternoon (2pm–5pm), because during each of those times, the meteorological conditions remain relative constant. This would result in 12 different transition matrices, where three matrices represent a typical day in each one of the four seasons (summer, winter, fall, and spring) of the year. Since a solar panel can only generate energy during daylight hours, it is assumed that the CGCS is only operational during daylight hours, as to avoid the need for large ESS capacity that would be required for night operation. Of course, the number of matrices collected per day H should be adjusted depending on the observed daily and seasonal variations in cloud coverage of the pertinent geographical location.

C. Energy Storage System Model

A general model for ESS is utilized that is not restricted to any particular energy storage technology. Accordingly, the ESS is mainly characterized by its *SOC*, which is a value within the range of [0, 1] that indicates the percentage of charged ESS' total energy capacity [26]–[28]. The ESS maximum energy capacity (kWh) is labeled as β_{ess}.

Furthermore, a discretized model for the ESS [29] is utilized, where the ESS *SOC* is divided into $L+1$ equally spaced levels: $\{B_0, B_1, \ldots, B_L\}$, where $0 \leq B_l \leq 1$. For the ESS *SOC* level $B_L = 0$, the ESS is completely depleted, while the ESS *SOC* level of $B_0 = 1$ corresponds to the fully charged state. Accordingly, it is assumed that $\delta_2 = \beta_{ess}(B_l - B_{l+1}) = \beta_{ess}/L$ for $0 \leq l \leq L - 1$. For simplicity, the B_l levels are defined in such a way that δ_2 is equal to the smallest possible transferrable energy to/from the ESS per timeslot, where a timeslot equals to τ as previously defined. As an example, δ_2 could be the energy (in kWh) stored in the ESS during one timeslot by a solar panel operating in the state G_7 (recall that G_7 is the solar radiation state that corresponds to the state of the smallest solar energy production). Under the above assumptions, the ESS charging/discharging is a deterministic process, and hence the transition probability from state l to state l' of ESS is going to depend on transition probabilities between solar radiation states (the energy generation rate) and the probability of EVs arrival and departure (the energy demand rate).

The ESS has an associated investment cost per kWh of ξ [$/kWh], which includes purchasing and installation costs. The ESS is also associated with a maintenance cost μ_e ($/kWh)

per year [7], [30]. Parameter γ is used to express the ratio of the ESS energy storage cost per kWh to the solar energy generation cost per kW; i.e.,$\gamma = (\xi + T\mu_e)/(\zeta + T\mu_k)$, where T is the system's planning horizon in years.

This approach of ESS modeling could be customized to fit the charging/discharging process of many different energy storage technologies, including energy storage methods with linear and nonlinear charging/discharging process, as well as a technology that requires a delay period before charging/discharging starts.

D. Queueing Model

A discrete-time Markov chain is considered with a discrete Poisson arrival process of EVs of intensity λ[arrivals/timeslot], where the timeslot duration τ is as previously defined. The utilized service time model is inspired in [31], which assumes different battery sizes and corresponding exponentially distributed EV service time. However, due to the current model being of discrete-time type, an analogous geometric service time distribution is assumed, driven by the randomness in the amount of energy needed by the EVs' batteries. The parameter d denotes the EV charging completion probability during a timeslot [32]. Therefore, d is the probability that an EV battery requires δ_1 kWh at the beginning of a timeslot, meaning that, if there is enough power, the EV battery will be fully charged at the end of the timeslot. In the discrete-time model, all state transitions (i.e., departure/arrival of EVs to/from the system, change of radiation levels, change of ESS's SOC) occur at the timeslot boundary. That is, for example, if an EV arrives in the middle of a slot, it will start charging only at the beginning of the next timeslot.

It is assumed that a server in the queueing model corresponds to a charging station with rate Y, so that each charging station can serve at most one EV at any given time. The charging system has a maximum of C_s installed charging stations. The challenge in analyzing the charging system's queueing model is that the number of operational servers/charging stations during a timeslot is a random variable that depends on the available insolation intensity G_r and on the ESS SOC. Note that in the current model, ESS discharges energy whenever the available solar radiation does not suffice to meet the EV demand. Additionally, the number of active charging stations cannot be greater than the number of EVs v in the charging system. Hence, given the number of solar panels K, the available solar power $\theta_r = K \cdot \rho_r$, the number of EVs in the system v, and ESS's SOC B_l, the number of operational charging stations during a timeslot is

$$N_{v,r,l} = \min(N_r + N_l, v, C_s) \qquad (5)$$

where $N_r = \theta_r/Y$ is the maximum number of charging stations that can be operated with the available solar power of θ_r, and $N_l = Cess \cdot B_l/(Y \cdot \tau)$ is the largest number of charging stations that can be powered by the available ESS energy. Hence, given v EVs in the system, the probability that g out of v EVs are fully charged within a timeslot is given by

$$\phi_{v,g} = \binom{N_{v,r,l}}{g} d^g (1-d)^{N_{v,r,l}-g}. \qquad (6)$$

It is noted that in case of a reduction in the number of operational charging stations $N_{v,r,l}$ due to a decline in solar radiation intensity and with lack of stored energy to compensate for this decline in the solar radiation, there is a possibility of service interruption of the charged EVs. However, since the change in $N_{v,r,l}$ happens at the timeslot boundary, the EV service time remains geometrically distributed. The suspension in service is reflected by a decrease in the system's charging completion probability in (6) due to decline in $N_{v,r,l}$.

In the current queueing system model, there is maximum queueing capacity of V EVs, which is set by the charging system operator (i.e., there is space for maximum of V EVs in the system). Once there are V EVs in the system, no more EVs can enter the system. The goal is to minimize the average number of blocked EVs, which corresponds to loss revenues to the charging system owner.

E. State Space and the Transition Probabilities

Each system state is represented by a tuple (v, r, l), where v ($0 \leq v \leq V$) is the number of EVs in the system, r ($0 \leq r \leq 8$) is the solar radiation state, and l ($0 \leq l \leq L$) is the ESS SOC. The transition probabilities from state (v, r, l) to state (v', r', l') are derived, where the system's one-step transition probability $P_{v',r',l'}^{v,r,l}$ refers to the probability of transitioning from state (v, r, l) to state (v', r', l') in one timeslot. Some of the state transition can be easily defined, for example:

$$P_{v+m,r,0}^{v,8,0} = \psi_{0,r} \Pr(m), \quad v+m < V$$
$$P_{V,r,0}^{v,8,0} = \psi_{0,r} \Pr(m \geq V - v) \qquad (7)$$

where $\Pr(m)$ is the probability of having m EV arrivals in a timeslot following a Poisson distribution with mean λ, and $\Pr(m \geq V - v)$ is the probability of having $V - v$ or more EV arrivals in a timeslot given a Poisson arrival process with mean λ.

For state transitions where the number of EVs varies and/or the solar radiation state varies, the ESS' SOC also changes depending on the need to charge/discharge energy from the ESS. For instance, an increase in number of EVs might require discharging the ESS to serve the arriving EVs, while an excess of the renewable energy due to a rise in solar intensity will start a charging process of the ESS. The transition probability from state (v, r, l) to state (v', r', l') is

$$P_{v',r',l'}^{v,r,l} = \psi_{r,r'} \sum_{|\min(0,h)| \leq m \leq v'} \Pr(m).\phi_{v,m+h} \qquad (8)$$

where $h = v - v', v' \neq V$, and $\phi_{v,g}$ is determined as shown by (6). In addition, since the change in ESS' SOC depends on the current solar state r and the number of EVs v, there is a restriction on the value of l', which has to corresponds either to l_1 or l_2 as (or otherwise $P_{v',r',l'}^{v,r,l} = 0$)

$$l_1 = \max\left(l - \left[(N_r - N_{v,r,l}) \cdot Y \cdot \frac{\tau}{\delta_2}\right], 0\right), N_r \geq \min(v, C_s)$$

$$l_2 = \min\left(l + \left[(N_{v,r,l} - N_r) \cdot Y \cdot \frac{\tau}{\delta_2}\right], L\right), N_r < \min(v, C_s).$$
$$(9)$$

When $v' = V$, the transition probability from state (v, r, l) to state (V, r', l') is

$$P_{V,r',l'}^{v,r,l} = \psi_{r,r'} \sum_{h \leq m \leq V} \Pr(m) \sum_{h \leq i \leq m} \phi_{v,i-h}$$
$$+ \psi_{r,r'} \Pr(m > V) \sum_{h \leq i \leq V} \phi_{v,i-h} \quad (10)$$

where $h = V - v$, l' is defined by (9), and Pr $(m > V)$ is the probability of having more than V EV arrivals in a timeslot. Additionally, there are transitions probabilities for which $P_{V,r',l'}^{v,r,l} = 0$, in the following.
1) $(r = 8) \wedge (l = 0) \wedge (v' < v)$, where $\wedge$ is the "and" operator (EVs cannot complete charging without energy).
2) $(l' \neq l_1) \wedge (l' \neq l_2)$ (i.e., l' does not indicate the correct ESS state).
3) $h = v' - v > N_{v,r,l}$ and $v' < v$ (there is not enough energy to completely charge h EVs).

The one-step transition matrix $\mathbf{Q}$ is defined with J columns and J rows, where $J = (V+1) \cdot (R+1) \cdot (L+1)$ and $R = 8$. The steady-state probability vector $\bar{\Pi} = [\tilde{\Pi}_0, \dots, \tilde{\Pi}_V]$, where $\tilde{\Pi}_v = [\Pi_{v,0}, \dots, \Pi_{v,R}]$, $\Pi_{v,r} = [\pi_{v,r,0}, \dots, \pi_{v,r,L}]$ and $\pi_{v,r,l}$ is the steady-state probability of being in the state (v, r, l). The rows and columns in the matrix $\mathbf{Q}$, which are numbered from 1 to J, have a one-to-one correspondence with the CGCS's states, which are ordered from $(0, 0, 0)$ up to (V, R, L), following the ordering of elements of the vector $\bar{\Pi}$. To determine the steady-state probabilities, the following equations are solved:

$$\bar{\Pi} = \bar{\Pi} \times \mathbf{Q}$$
$$\sum_{v,r,l} \pi_{v,r,l} = 1. \quad (11)$$

F. Performance Measures and the Sizing Problem

The queueing theory performance metrics are utilized to evaluate the performance of the EV charging system. The expected number of EVs at the charging system is

$$E[V] = \sum_{0 \leq v \leq V} \tilde{\Pi}_v \cdot v \cdot e \quad (12)$$

where e denotes an identity column vector of size $(R+1) \times (L+1)$. The average number of EVs that leaves the charging system per timeslot, or the average system throughput per slot, is determined by

$$\bar{\alpha} = \sum_{0 \leq v \leq V} \sum_{0 \leq r \leq R} \sum_{0 \leq l \leq L} \pi_{v,r,l} \left(\sum_{0 \leq g \leq N_{v,r,l}} g \cdot \phi_{v,g} \right) \quad (13)$$

where $\phi_{v,g}$ is a given in (6). The blocking probability P_{bl} denotes the fraction of EVs unable to enter the charging system and can be obtained from the average throughput as in

$$P_{bl} = 1 - (\bar{\alpha}/\lambda). \quad (14)$$

By Little's law, the average delay time (in timeslots) per EV is

$$D = E[V]/\bar{\alpha}. \quad (15)$$

The average delay is an important performance measure for the overall performance of the charging system, as the sizing problem seeks to determine the optimal number of solar panels K and the size of ESS $Cess$, such that the target EV delay D_{td} [timeslots] is not exceeded. As the atmospheric conditions vary per season and per time-of-day, the charging system's delay is evaluated for each time-of-day period h ($1 \leq h \leq H$) and for each season s($1 \leq s \leq 4$) of the year to ensure that the target delay is met at all times. Hence, $D_{h,s}$ is the average delay [timeslots] per EV found by evaluation (15) for period h of season s. The goal of the sizing problem is to minimize the total costs throughout the planning period as shown in (16), where t is the year index. The formula $W = (1 + U)^{-(t-1)}$ is used as the present-worth value coefficient [33], where U is the discount rate. More specifically, W is used to adjust the future maintenance cost to the present value by incorporating discount rates in the present-worth cost [20]. The same present-worth factor W is assumed for the solar panels and for the ESS, although this could be easily changed if needed. T is the total number of years in the planning horizon (e.g., hardware retention time). Thus, the overall optimization problem formulation is

$$\min Cost(K, \beta_{\text{ess}}) = K \cdot \omega \left(\zeta + \sum_{1 \leq t \leq T} W \cdot \mu_k \right)$$
$$+ \beta_{\text{ess}} \left(\xi + \sum_{1 \leq t \leq T} W \cdot \mu_e \right)$$
$$s.t \; D_{h,s} \leq D_{\text{td}}, \quad 1 \leq s \leq 4, \; 1 \leq h \leq H. \quad (16)$$

IV. Search-Based Algorithm

The EV average delay as a function of the number of solar panels and the ESS capacity is a highly complex and nonlinear problem [34], making (16) hard to solve even as a nonlinear integer programming problem. For such complex problems, search techniques have been proven to be effective in finding optimal or near optimal solutions [35]. Accordingly, a search-based algorithm is devised to efficiently explore the problem's solution space. A solution in the search space is characterized by two parameters $[K, \beta_{\text{ess}}]$, where K is the number of solar panels and β_{ess} is the ESS capacity. The search-based algorithm seeks to find a solution $[K_{\text{opt}}, \beta_{\text{opt}}]$ that leads to the minimum system planning cost, while meeting the predetermined EV target delay, D_{td}. It was also noted that it is only necessary to evaluate D_{td} for the seasonal time-of-day h_w that produced the smallest average solar energy, since a solution that could meet D_{td} during h_w would necessarily be able to meet D_{td} in any other period as well. Hence, as a first step, the search-based algorithm determines the h_w period utilizing the transition probability matrices $\mathbf{\Psi}_{h,s}$, where h is the time-of-day index and s is the season index. The complete search algorithm is outlined as Algorithm I in the flowchart in Fig. 2.

The first step in obtaining a solution is to bound the search space. The upper bound on the number of solar panels was first established as follows. The geometric distribution
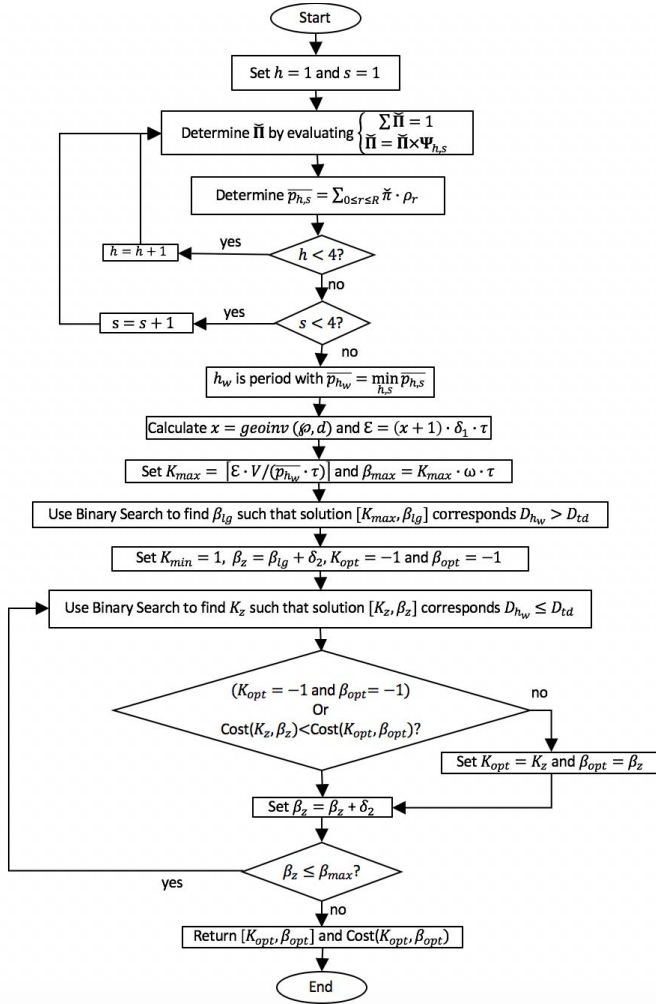
Fig. 2. Algorithm I.

TABLE II
ENERGY RESOURCES PARAMETERS

Solar Panel Parameters	ESS Parameters
Area (m^2) = 50 Efficiency = 1 Max Power Capacity (kW) = 50 Investment cost ($/kW) = 200 Annual Maintenance cost ($/kW) = 20	Charging/discharging Efficiency = 1 δ_2 = 10 kWh Energy rating cost ($/kWh) = 200 Annual Maintenance cost ($/kWh) = 20

empty. Hence, the upper bound on the ESS capacity is set to $K_{\max} \cdot \omega \cdot \tau$ kWh. Setting upper bounds for the number of solar panels and ESS capacity restricts the solution space, which allows the search-based algorithm to find the optimal solution faster.

In order to effectively search the solution space, the space is further bounded from below as follows. The algorithm starts by finding the largest ESS capacity β_{lg}, such that $[K_{\max}, \beta_{lg}]$ leads to $D_{h_w} > D_{\text{td}}$ for the period with the least average solar power generation h_w, where D_{h_w} is found as in (15) by evaluating the Markov chain for h_w. The *Binary Search* method [36] is utilized in order to find such a β_{lg} in the most efficient way. Finding β_{lg} allows to disregard all solutions where $\beta_{\text{ess}} \leq \beta_{lg}$ regardless of the number of solar panels, since as $[K_{\max}, \beta_{lg}]$ does not satisfy D_{td} then no solution with $\beta_{\text{ess}} < \beta_{lg}$ will be able to meet the D_{td} requirement. For each ESS capacity β_{ess} in the interval $[\beta_{lg} + \delta_2, \beta_{\max}]$, the search-based algorithm finds the minimum value of K that satisfies D_{td} using the *Binary Search* method; clearly, this will correspond to the minimum cost solution given this ESS capacity. In order to determine whether a solution meets D_{td}, the Markov chain analysis is used to obtain the average EV delay D_{h_w} for period h_w. The ESS capacity is always incremented by δ_2, since an increment that is less than δ_2 will not change the ESS state. The optimal solution is the $[K, \beta_{\text{ess}}]$ pair that corresponds to the minimum planning cost, while also satisfying the D_{td} requirement.

V. CASE STUDY

A. Case Study Parameters

To illustrate the use of the described methodology, a numerical example is presented in this section. In this example, the solar radiation's state $r = 0$ matches the maximum solar radiation intensity of 1 kW/m^2. The other solar panels' parameters are shown in Table II, including the investment and maintenance costs. With a maximum capacity of 25 kW per solar panel, the solar states $r = 0, \ldots, 8$ corresponds to the output power values of $G_0 = 25$ kW, $G_1 = 21.875$ kW, $\ldots, G_7 = 3.125$ kW, and $G_8 = 0$ kW per solar panel. In this example, $Y = 25$ kW is the charging power per charging station. δ_1 is set to 10 [kWh], which corresponds to EV charging demand levels of: $C_0 = 0$ [kWh], $C_1 = 10$ [kWh], $C_2 = 20$ [kWh], *etc.* In this way, the charging completion probability d corresponds to the probability that EV demand equals 10 [kWh]. The timeslot duration is found as $\tau = (C_{i+1} - C_i)/Y$, which is equal to 0.4 h or 24 min. The ESS parameters are shown in Table II, which also include

service process models the number of timeslots an EV have to wait in the system before it is fully charged; it can also be viewed as "the number of failures to depart," which can be interpreted as the number of energy quanta needed before an EV is fully charged. $geoinv(\wp, \text{d})$ is defined as the inverse of cumulative distribution of the geometric service time and $\wp$ is a probability value. Then $x = geoinv(\wp, \text{d})$ is the number of energy quanta that at least $\wp \cdot 100\%$ of the arriving EVs have to receive from the charging stations before they are charged and depart. Ideally, $\wp$ should be set to 1 to account for the energy demand distribution of all EVs, but that would give $x = \infty$, which would not be practical; rather, $\wp$ is set to a value that is very close to 1, for example $\wp$ can be set to 0.9999. The maximum observed energy demand per EV for $\wp \cdot 100\%$ of the arriving EVs can be found as $\varepsilon = (x + 1) \cdot \delta_1 \cdot \tau$ (the +1 accounts for the timeslot during which the EV departs). It is then argued that the maximum energy the system would require is when its queue is full and all EVs' demand equals to ε. In this case, the system requires $K_{\max} = \lceil \varepsilon \cdot V / (\bar{p}_{h_w} \cdot \tau) \rceil$ solar panels, utilizing the smallest average solar energy produced per solar panel $\bar{p}_{h_w}$. Similarly, in the worst case, the ESS would have to save the energy produced by $K_{\max}$ solar panels operating at their maximum capacity, assuming the system's queue is

the investment and maintenance costs per kWh of ESS. The maximum ESS' *SOC* level depends on the ESS maximum energy storage capacity *Cess*; that is $L = Cess/\delta_2$.

The example utilizes the weather condition in Gothenburg, Sweden, based on the historic records from 1973 to 1999 [21]. The transition probabilities were estimated, as shown in (2). The example considers the transition matrix shown in (17) as the time-of-day period h_w with the least solar generation in the above geographical location [21]. As described in the Algorithm I in Section IV, the 3-D transition matrix in (11) will be simulated only for this period h_w with lowest average solar energy and the average EV charging delay will be calculated to ensure that target average delay is met. The example also considers a planning horizon of 20 years ($T = 20$) and a discount rate $U = 0.12$, which are used to evaluate the objective function

$$\Psi_1 = \begin{pmatrix}
53.8 & 22.5 & 7.1 & 4.7 & 2.7 & 2.3 & 1.7 & 2.6 & 2.6 \\
15.5 & 45.5 & 14.0 & 9.1 & 4.3 & 3.7 & 3.2 & 3 & 1.5 \\
7 & 24.5 & 23.4 & 15.3 & 8.8 & 7.2 & 6.2 & 5.4 & 2.2 \\
3.8 & 13.4 & 17.7 & 20.3 & 12.6 & 10.6 & 9 & 9.1 & 3.4 \\
2.2 & 8.5 & 12.1 & 15.9 & 16.2 & 14.4 & 13.4 & 13.2 & 4.2 \\
1.5 & 5.1 & 8.1 & 12.2 & 12.6 & 17.3 & 18.7 & 18.3 & 6.2 \\
1 & 3 & 5.2 & 7.4 & 9.5 & 14.2 & 22.2 & 28 & 9.5 \\
0.6 & 2 & 2.3 & 3 & 3.9 & 6.3 & 11.3 & 50.3 & 20.4 \\
0.5 & 0.7 & 0.8 & 1.1 & 1.3 & 2 & 3.8 & 13.5 & 76.3
\end{pmatrix}. \quad (17)$$

B. Simulation Results

First, the presented Markov chain model is validated by comparing the results of the Markov chain evaluation with the results of a simulated CGCS system (with the weather parameters defined in Section V-A). The EV arrival process follows a Poisson distribution process with the rate of λ [EVs/timeslot], where a timeslot corresponds to 24 min, as define above. Accordingly, the energy demand per EV is discretized into equal-sized quanta, where an energy demand quantum equals to 10 [kWh]. The energy demand (kWh) per EV is generated according to a geometric distribution with success parameter $d = 0.5$. That is, $d = 0.5$ is the charging completion probability in a timeslot, which equals the probability of an incoming EV having energy demand of 10 [kWh].

Using the solar states transition matrix in (17), a matrix of cumulative transition probabilities Ω is generated, such that $\Omega_{i,j} = \sum_{0 \le k \le j} \psi_{i,k}$. The charging system begins in a randomly chosen solar state r. The solar state r' in the next timeslot is chosen as follows: a uniformly distributed random number ϱ is chosen from interval $(0, 1)$; the next solar state r' corresponds to the state with the smallest index j ($r' = j$) such that $\Omega_{i,j} \ge \varrho$. The charging system was simulated for a total of $100\,000$ timeslots to guarantee convergence of the simulation results. The observed EV average delay, average number of EVs (average number of EVs in the system in a timeslot), and system throughput (the number of departures per timeslot) were recorded. The comparison results mainly focus on the
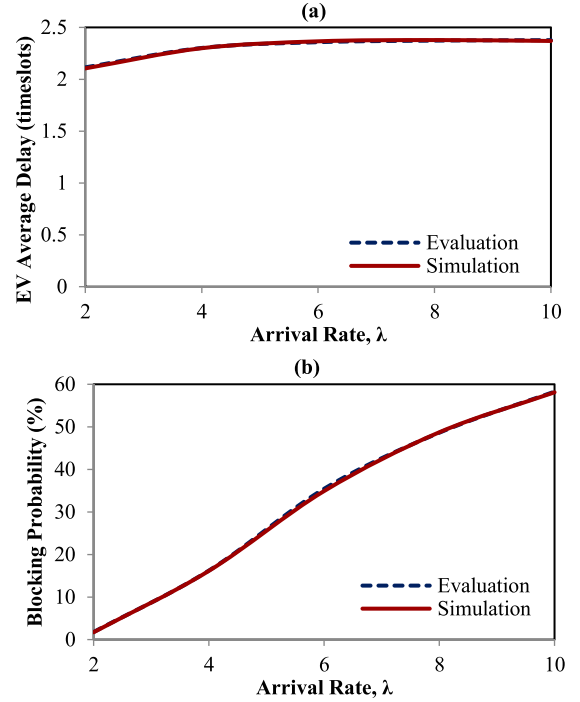

Fig. 3. (a) Average EV delay as arrival rate λ varies. (b) Blocking probability as arrival rate λ varies.

EV average delay, as this is the main performance measure used in the sizing problem.

Fig. 3(a) compares the evaluation and simulation results for the EV average delay as a function of the EV arrival rate λ, given 50 solar panels, $\beta_{\text{ess}} = 500$ kWh, and $C_s = V$ (the number of installed charging stations equals to the maximum number of EVs that can be queued in the system). As seen from Fig. 3, the Markov chain evaluation results closely follow the simulated results, registering a difference of no more than for 1%. The same results' accuracy was observed for the blocking probability [shown in Fig. 3(b)], the throughput, and the average number of EVs ($E[V]$). Results of no more than 3% difference for the EV average delay, the throughput, and the average number of EVs were observed, when the number of solar panels, ESS capacity, and the system queue capacity were varied for the simulated system and for the Markov chain model. These results demonstrate that the Markov chain model is a close approximation for the EV charging system, validating the solution methodology.

C. Evaluation Results

1) Search-Based Algorithm Results: The minimum cost solutions returned by the search-based algorithm is now considered, given $d = 0.5$, $\lambda = 1.5$, $C_s = V$, $D_{\text{td}} = 2$, and $V = 6$. The upper bounds on the solution space were first defined as shown in Algorithm I with $\wp = 0.998$ resulting in $K_{\max} = 148$ and $\beta_{\max} = 1480$. The obtained β_n values are within the interval [640, 1480]; that is $\beta_{lg} = 630$ kWh is the largest ESS capacity, such that $[K_{\max}, \beta_{lg}]$ leads to $D_{h_w} > D_{\text{td}}$ for period h_w, where D_{h_w} is found by evaluating (15) for the period h_w. As expected and depicted in Fig. 4, the solar panels capacity decreases as β_{ess} grows. However, the system's
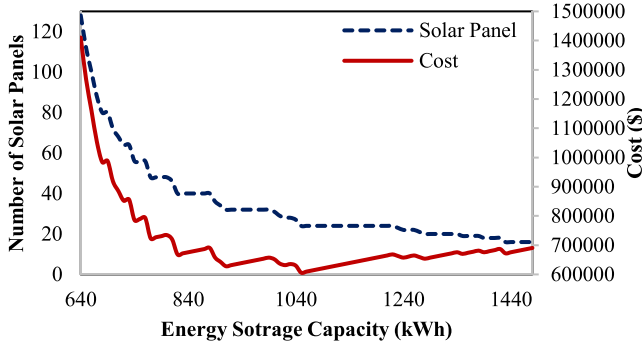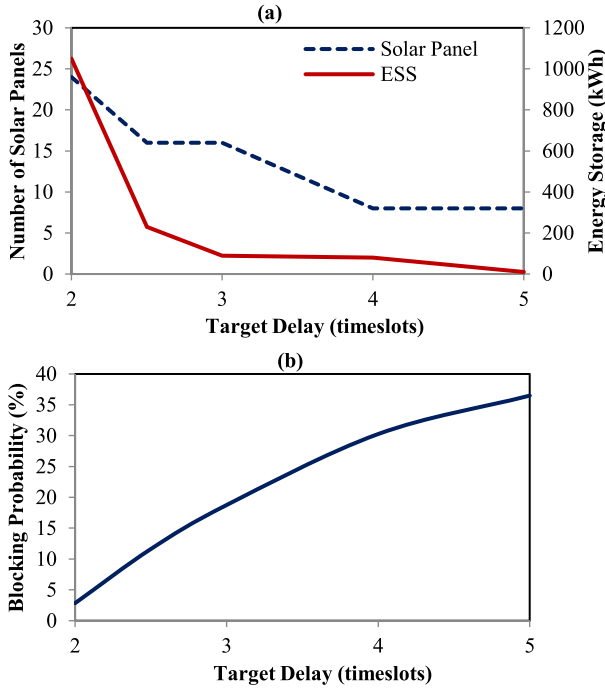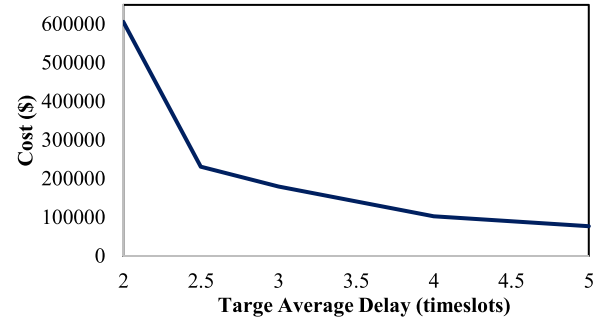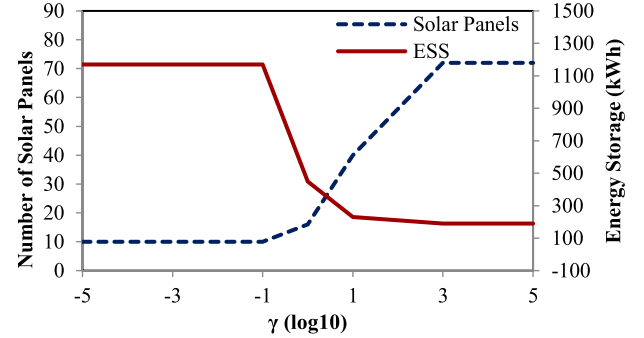
Fig. 4.   Number of solar panel and system costs as ESS capacity varies.

Fig. 5.   (a) Solar panel and ESS capacity as D_{td} varies. (b) Blocking probability as D_{td} varies.

Fig. 6.   System investment cost as D_{td} varies.

Fig. 7.   Solar panel and ESS capacity as γ varies.

investment cost does not increase or decrease monotonically as the ESS capacity or/and number of solar panels rise or decline, respectively. Consequently, the optimal solution is the minimum cost point of the system cost curve in Fig. 4, which corresponds to the pair of [24, 1050] (in Solar Panels and kWh, respectively) for this example case. The blocking probability for the optimal solution is 2.84%.

2) Varying Target Average Delay: This section analyzes how the optimal solar panels' capacity and the ESS capacity vary as a function of the target average EV delay. The system parameters are set as follows: $d = 0.5$, $\lambda = 1.5$, $C_s = V$, and $V = 6$. As expected, Fig. 5(a) shows that the optimal number of solar panels and the ESS maximum capacity decreases as the target EV delay increases. This is intuitive, since as the EVs are allowed to spend more time in the charging system, the charging system can benefit from utilizing its resources over longer time to meet the target average delay per EV. This result is mirrored in Fig. 6, which shows that the CGCS investment cost decreases with the increase in the target average delay. As expected, Fig. 5(b) shows that the

system's blocking probability, or the portion of EVs unable to enter the system, rises as D_{td} increases. That is, as the EVs are allowed to spend more time at the charging system (i.e., as D_{td} grows), more arriving EVs find the system's queue full, and this in turn increases the system's blocking probability.

On the other hand, as the target average delay per EV decreases, the number of solar panels and the ESS capacity increase in order to allow for a fast EV charging. For this particular evaluation case, the minimum possible average delay per EV is $D = 2$. Accordingly, as D_{td} approaches 2, the ESS capacity and the number of solar panels capacity increase in order to raise the probability of having enough energy to charge the arriving EVs.

3) Varying γ: In Fig. 7, the ratio between the cost per kWh of ESS and the cost per kW of solar energy is varied from 10^{-5} up to 10^5, while $D_{td} = 2.2$, $d = 0.5$, $\lambda = 1.5$, $C_s = V$, and $V = 6$. Whenever $\gamma = 10^{-1}$, the ESS is significantly cheaper than the solar energy production, so that the ESS capacity is greatly augmented in order to reduce the investment in solar panels. In other words, a large ESS capacity stores more energy, allowing for greater variations in the power generated by the solar panels, which in turn reduces the required solar panel capacity.

Sufficiently large stored energy allows the charging system to compensate for the power generation fluctuations in the solar radiation. Accordingly, it was observed that the ESS capacity cannot be less than 190 kWh even as γ rises, which explains why the ESS and solar panel capacity stabilizes once $\gamma \geq 10$. As the other system's characteristics do not change as γ varies beyond this limit, the charging system's EV blocking probability stays around 7% even as γ grows. Similarly, as the solar panels are the only source of energy, their number cannot be smaller than 10 solar panels even as
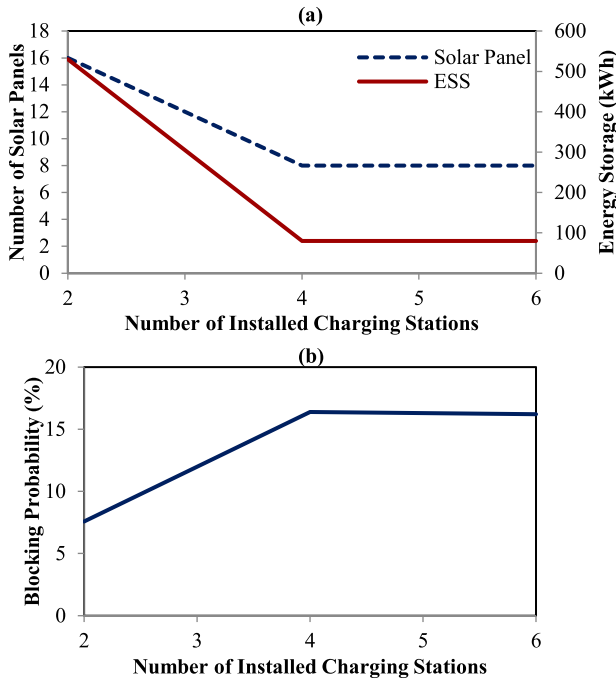
Fig. 8. (a) Solar panel and ESS capacity as d varies with $D_{td} = 2.2$. (b) Blocking probability as d varies with $D_{td} = 2.2$.
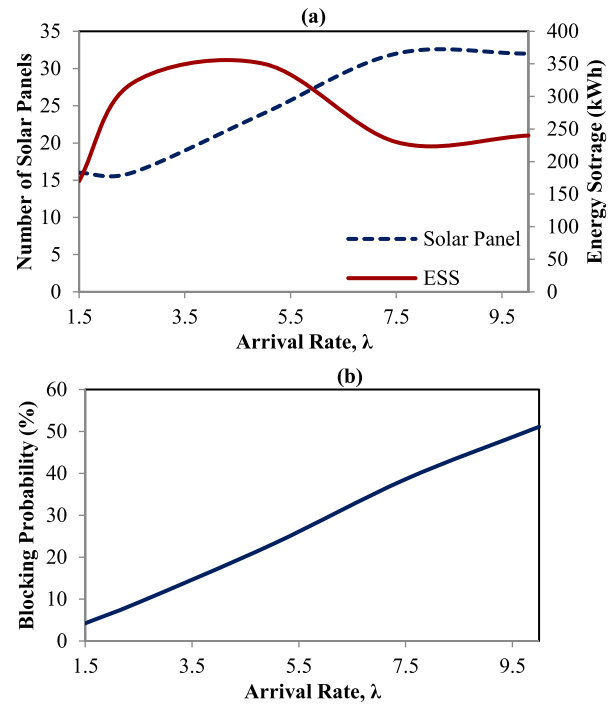

Fig. 9. (a) Solar panel and ESS capacity as λ varies. (b) Blocking probability as λ varies.

they become more expensive than the ESS. This explains why the solar panels' optimal capacity also flattens for $\gamma \leq 0.1$.

4) Varying EV Departure Probability: In this section, the EV departure probability d is varied, while maintaining the arrival rate $= 1.5$, $C_s = V$, and $V = 6$. As d decreases, a larger fraction of the arriving EVs requires less than 10 [kWh] to be fully charged. Accordingly, a rise in d corresponds to a decrease in charge demand per EV, which explains the drop in the number of solar panels and the ESS capacity in Fig. 8(a) as d increases. It was also observed that the charging system cannot satisfy the target average delay $D_{td} = 2.2$ when $d < 0.5$. However, when $D_{td} = 5$, it was possible to find solutions for $d \geq 0.2$. It is concluded that as the EV charging demand intensifies (as d decreases), a rise in target delay D_{td} permits the charging system to accommodate more EV load demand. As the electric demand per EV decreases with an increase in d, the charging system requires less resources to meet $D_{td} = 2.2$. However, the decrease in solar panels and ESS capacity, due to the rise in d, results in a rise in blocking probability, as shown in Fig. 8(b).

5) Varying Arrival Rate λ: In this section, the arrival rate λ is varied, while maintaining the queueing capacity $V = 10$, $C_s = V$, $d = 0.7$, and $D_{td} = 2$. As expected, the energy resource capacity generally grows as the average number of arriving EVs increases with λ, as shown in Fig. 9(a). When $\lambda > 5$, the system gets saturated, so that the average queue length stops increasing significantly (staying bounded at 10 EVs). Accordingly, though the number of solar panels augments to meet the growing arrival of EVs, the average queue length does not increase so as to require an increase in ESS capacity. In fact, the increase in the number of solar panels alleviates some of the randomness effects of the arrival process, allowing to satisfy the demand with actually

less ESS capacity. This is why the ESS curve exhibit the nonmonotonous behavior in Fig 9(a), starting to decrease for $\lambda > 5$. In contrast, if the queue capacity is designed to be greater or equal to 2λ, both the solar panels and ESS capacity continue to grow monotonically as λ rises. The average queue length increases with λ, leading to the rise in the blocking probability as λ grows [Fig. 9(b)].

Similar to the above results, when the system's queueing capacity V grows, the charging system has to also increase the energy resource capacity (solar panels and ESS) in order to handle the growing energy demand due to the rise in the number of EV that can enter the system. As expected, the blocking probability decreases as V rises, since more EV are able to enter the charging queue.

6) Varying the Number of Installed Charging Stations: This section analyzes how the optimal energy resources capacities change as the number of installed charging stations C_s varies, with $V = 6$, $d = 0.8$, and $D_{td} = 2.36$. A rise in C_s allows to reduce the charging's systems average queue length, and this explains the decrease in number of solar panels and the ESS capacity as C_s grows [Fig. 10(a)]. However, a drop in energy resources capacity leads to a slight increase in the overall system blocking probability, as depicted in Fig. 10(b).

7) Varying ω: In this section, the maximum generating capacity per solar panel ω is varied, while maintaining the arrival rate $= 1.5$, $C_s = V$, $d = 0.5$, $D_{td} = 2.2$, and $V = 6$. As anticipated, Fig. 11 illustrates that the rise in maximum generating capacity per solar panel leads to a decline in the optimal number of solar panels required by the system. In particular, when ω doubles from 25 to 50 kW, the optimal number of solar panels is reduced to half from 16 solar panels to 8 solar panels. As the EVs' demand characteristics (arrival rate, departure probability, and queue capacity) do not change,
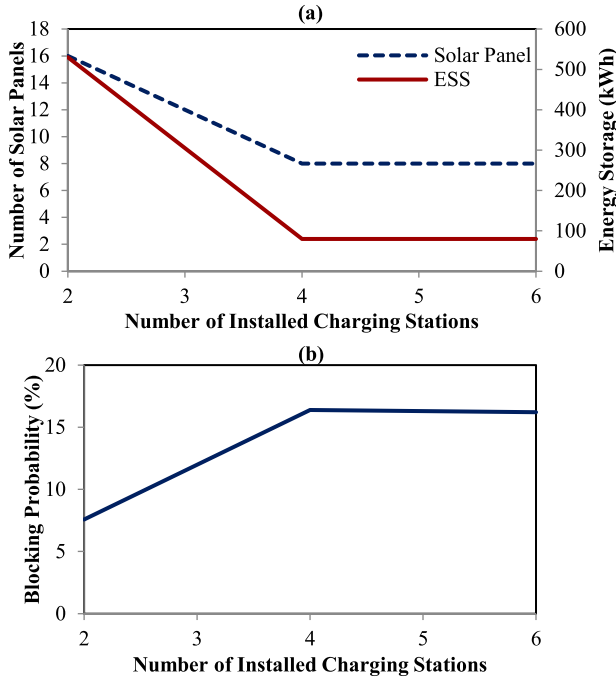
Fig. 10.　(a) Solar panel and ESS capacity as C_s varies. (b) Blocking probability as C_s varies.
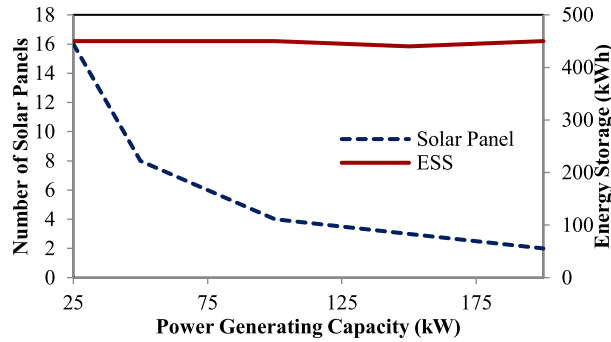

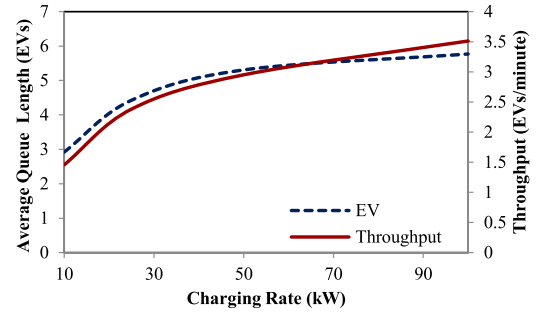Fig. 11.　Solar panel and ESS capacity as ω varies.

Fig. 12.　Average number of EVs and throughput as Y varies.
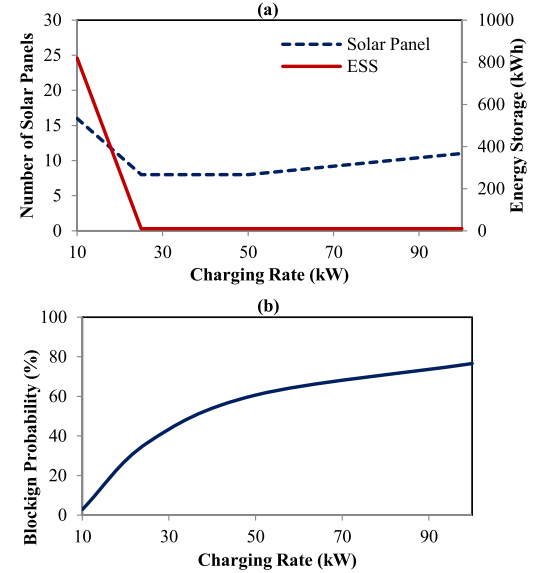
Fig. 13.　(a) Solar panel and ESS capacity as Y varies. (b) Blocking probability as Y varies.

the ESS capacity does not change. Similarly, the system blocking probability remains around 6.5%.

8) Varying the Charging Rate: This section illustrates how the number of solar panels and the ESS capacity change as the power rate (kW) per charging station Y is varied, while maintaining the arrival rate $\lambda = 1.5$, $C_s = V$, $d = 0.7$, $V = 6$, and $D_{td} = 90$ min. As Y changes, the timeslot duration τ also varies. In particular, $\tau = 60$ min for $Y = 10$ kW, while $\tau = 6$ min for $Y = 100$ kW. As expected, the system's throughput increases as Y grows (Fig. 12), and this allows meeting the target averaged delay of 90 min with less resources. This in turn explains the declined in the energy resources capacity, as indicated in Fig. 12(a). In particular, as the rate of solar energy use increases with Y, the need to store energy also declines. This explains the significant drop in ESS capacity as Y increases [Fig. 13(a)]. However, as the number of solar panels and the ESS capacity decrease with Y, the average queue length grows, as shown in Fig. 12. Accordingly, more EVs are unable to enter the system, and this justifies the rise in blocking probability as Y grows [Fig. 13(b)].

VI. IMPLEMENTATION OF THE CGCS METHODOLOGY

This section summarizes the necessary steps to implement the methodology for the sizing of a CGCS presented in this paper. The goal of the proposed methodology is to appropriately size the energy-generating resources (solar panels, in the case analyzed in this paper) and the energy storage resources, as to minimize the investment cost, while ensuring the required level of performance (average EC charging time, in the case analyzed in this paper).

First, the designer should characterize the EV fleet served by the CGCS. The recorded EV fleet attributes include the EV arrival rate per unit of time and the maximum and minimum energy demand per EV. The CGCS planner should obtain the physical characteristics of the future CGCS. This includes the number of installed charging stations and the power rate per charging station, the maximum power capacity, the area size and efficiency per solar panel, as well as the CGCS' maximum queue capacity, which limits the number of EVs that can be in the system at any time. The CGCS planner should also specify the ESS technology to be used, as this will influence the attributes of the ESS model. Additionally, the CGCS sizing problem requires knowledge of the ESS' investment cost per kWh and annual maintenance cost per kWh, as well as solar panels' investment cost and yearly maintenance cost per kW. The maintenance costs are incurred throughout

the CGCS' expected lifetime or planning horizon, which should also be specified.

To model the energy demand per EV, one should specify the EV energy demand quantum, which is the number of kWh transferred to an EV per timeslot. As previously shown (Section III), the timeslot duration is calculated by dividing the EV energy demand quantum by the power rate per charging station and is used in to analyze/evaluate the future CGCS. One should note that the ESS quantum is the minimum number of kWh charged/discharged to/from the ESS per timeslot.

The CGCS system model accounts for the randomness in solar power generation, which is driven by the unpredictably of the solar radiation. The variation in solar radiation intensity is influenced by the local cloud coverage, and, as such, cloud coverage data for the CGCS' location, or for a location with similar meteorological conditions, need to be obtained. In practice, cloud coverage data can be easily obtained through measurements, without requiring expensive apparatus [21]. Since each cloud coverage level corresponds to a solar radiation state [as per (1)], one can determine the solar state-transition probabilities by recording the number of transitions among the different cloudiness levels occurring during one-hour period (Section III-B). Multiple solar radiation transition matrices should be generated, depending on the time-of-day and seasonal variations observed. Accordingly, a system state is described by the solar radiation state, number of EVs, and the *SOC* of the ESS.

The CGCS service time model should be characterized. Due to assumed distribution of EV battery sizes, this paper assumed a geometric distributed service time model with a success probability equal to the probability that an EV gets fully charged after one timeslot. The value for the charging completion probability indicates the fraction of EVs that only require one quantum of energy within a timeslot and can be obtained from the observed energy demand levels of the EV fleet. The CGCS designer should also define the system's energy management policy, which dictates how the solar energy and the energy stored by the ESS are utilized. This energy consumption policy influences the transition probability among the CGCS system states (see Section III-E).

Finally, the solution to the sizing problem also depends on the target performance measure of the CGCS. This paper considered this measure to be the target average delay per EV, which is the average number of timeslots necessary to fully charge an EV. The target average delay is set by the CGCS' operator and is influenced by the intended use of the CGCS; e.g., if the CGCS is used by office employees, the target delay per EV will typically be on the order of a duration of a business day and will be longer than when the CGCS is in a mall parking lot, in which case the target delay per EV will be on the order of an average customer's shopping time. Both of these scenarios will be longer than when the CGCS is used as a conventional gas station, in which case the target delay per EV could be on the order of few minutes. Other metrics, such as the system's utilization and throughput, can also be used to characterize the system's performance. Furthermore, it is possible to extend the current methodology to accommodate

priorities in the serving order of the EVs; e.g., an EV of a customer who intends to spend only a short time shopping could be given higher priority than a customer who intends to shop for longer time.

With the above data, one can model the CGCS using afore-described 3-D Markov chain model and formulate the sizing problem as described in Section III. Once the problem is formulated, the solution algorithm presented in Section IV can be applied to find the optimal number of solar panels and the optimal ESS capacity that meets the target CGCS' performance measure.

VII. Conclusion

This paper studies the optimal planning problem for a completely green EV charging system, such as one which is situated in a green village, whose energy is generated exclusively by solar panels. The goal was to design a methodology for determining the optimal number of solar panels and the optimal ESS capacity that minimize the charging system's investment costs while satisfying a specified target average charging delay of an EV. The solar panels' output power is driven by the solar radiation, which is represented by a discrete Markov chain model and is affected by the local cloud coverage. The transition probability from one solar radiation state to the next is determined by the number of transition in the corresponding cloudiness levels within one-hour period. Accordingly, the methodology relies on a 3-D Markov chain model, in which each state is characterized by the solar radiation state, the number of EVs in the system, and the ESS *SOC*. A search-based algorithm was designed to efficiently explore the solution space of the formulated nonlinear integer programming problem in order to find an optimal solution. The system's model was validated by simulations. The use of the methodology was demonstrated by a simple example. From the evaluation results of the example, it was observed that the optimal number of solar panels and the ESS capacity depend mostly on the system's queueing capacity and the number of installed charging stations, which determine the system's throughput and the average number of EVs, and which in turn determine the overall EV average delay. The evaluation results also showed that, as expected, the optimal number of solar panel and the ESS capacity decreased with the increase in the target average delay, the EV charging completion probability, the number of installed charging stations, and the power rate per charging station. The presented methodology could be easily extended to accommodate more complex scenarios, such as different priorities assigned to customers and different policy of the use of the energy storage (see Section III), for example. Other possible extensions include a model in which EV can leave a CGCS after being only partially charged, with a reward depending on the average charge delivered during a visit to a CGCS.

References

[1] F. Mwasilu, J. J. Justo, E.-K. Kim, T. D. Do, and J.-W. Jung, "Electric vehicles and smart grid interaction: A review on vehicle to grid and renewable energy sources integration," *Renew. Sustain. Energy Rev.*, vol. 34, pp. 501–516, Jun. 2014.

[2] G. H. Fox, "Electric vehicle charging stations: Are we prepared?" *IEEE Ind. Appl. Mag.*, vol. 19, no. 4, pp. 32–38, Jul./Aug. 2013.

[3] P. Sadeghi-Barzani, A. Rajabi-Ghahnavieh, and H. Kazemi-Karegar, "Optimal fast charging station placing and sizing," *Appl. Energy*, vol. 125, pp. 289–299, Jul. 2014.

[4] A. Mohsenzadeh, C. Pang, S. Pazouki, and M. Haghifam, "Optimal siting and sizing of electric vehicle public charging stations considering smart distribution network reliability," in *Proc. North Amer. Power Symp. (NAPS)*, 2015, pp. 1–6.

[5] G. Wang, Z. Xu, F. Wen, and K. P. Wong, "Traffic-constrained multiobjective planning of electric-vehicle charging stations," *IEEE Trans. Power Del.*, vol. 28, no. 4, pp. 2363–2372, Oct. 2013.

[6] Z.-J. Pan and Y. Zhang, "A novel centralized charging station planning strategy considering urban power network structure strength," *Electr. Power Syst. Res.*, vol. 136, pp. 100–109, Jul. 2016.

[7] S. Negarestani, M. Fotuhi-Firuzabad, M. Rastegar, and A. Rajabi-Ghahnavieh, "Optimal sizing of storage system in a fast charging station for plug-in hybrid electric vehicles," *IEEE Trans. Transport. Electrific.*, vol. 2, no. 4, pp. 443–453, Dec. 2016.

[8] C. J. R. Sheppard, A. Harris, and A. R. Gopal, "Cost-effective siting of electric vehicle charging infrastructure with agent-based modeling," *IEEE Trans. Transport. Electrific.*, vol. 2, no. 2, pp. 174–189, Jun. 2016.

[9] O. Arslan and O. E. Karaşan, "Energy management in microgrids with plug-in electric vehicles, distributed energy resources and smart home appliances," in *Plug In Electric Vehicles in Smart Grids*. Singapore: Springer, 2015.

[10] P. J. Tulpule, V. Marano, S. Yurkovich, and G. Rizzoni, "Economic and environmental impacts of a PV powered workplace parking garage charging station," *Appl. Energy*, vol. 108, pp. 323–332, Aug. 2013.

[11] S. Bahramirad, W. Reder, and A. Khodaei, "Reliability-constrained optimal sizing of energy storage system in a microgrid," *IEEE Trans. Smart Grid*, vol. 3, no. 4, pp. 2056–2062, Dec. 2012.

[12] H. Liang and W. Zhuang, "Stochastic modeling and optimization in a microgrid: A survey," *Energies*, vol. 7, no. 4, pp. 2027–2050, 2014.

[13] H. N. T. Nguyen, C. Zhang, and J. Zhang, "Dynamic demand control of electric vehicles to support power grid with high penetration level of renewable energy," *IEEE Trans. Transport. Electrific.*, vol. 2, no. 1, pp. 66–75, Mar. 2016.

[14] C. Le Floch, F. Belletti, and S. Moura, "Optimal charging of electric vehicles for load shaping: A dual-splitting framework with explicit convergence bounds," *IEEE Trans. Transport. Electrific.*, vol. 2, no. 2, pp. 190–199, Jun. 2016.

[15] V. del Razo, C. Goebel, and H.-A. Jacobsen, "Vehicle-originating-signals for real-time charging control of electric vehicle fleets," *IEEE Trans. Transport. Electrific.*, vol. 1, no. 2, pp. 150–167, Aug. 2015.

[16] D. P. Birnie, "Solar-to-vehicle (S2V) systems for powering commuters of the future," *J. Power Sour.*, vol. 186, no. 2, pp. 539–542, Jan. 2009.

[17] H.-M. Neumann, D. Schär, and F. Baumgartner, "The potential of photovoltaic carports to cover the energy demand of road passenger transport," *Prog. Photovolt. Res. Appl.*, vol. 20, no. 6, pp. 639–649, Sep. 2012.

[18] G. R. C. Mouli, P. Bauer, and M. Zeman, "System design for a solar powered electric vehicle charging station for workplaces," *Appl. Energy*, vol. 168, pp. 434–443, Apr. 2016.

[19] E. Park and S. J. Kwon, "Renewable electricity generation systems for electric-powered taxis: The case of Daejeon metropolitan city," *Renew. Sustain. Energy Rev.*, vol. 58, pp. 1466–1474, May 2016.

[20] E. Hajipour, M. Bozorg, and M. Fotuhi-Firuzabad, "Stochastic capacity expansion planning of remote microgrids with wind farms and energy storage," *IEEE Trans. Sustain. Energy*, vol. 6, no. 2, pp. 491–498, Apr. 2015.

[21] J. S. G. Ehnberg and M. H. J. Bollen, "Simulation of global solar radiation based on cloud observations," *Solar Energy*, vol. 78, no. 2, pp. 157–162, 2005.

[22] J. Ehnberg, "Autonomous Power Systems based on Renewables - On generation reliability and system control," Ph.D. dissertation, Dept. Energy Environ., Chalmers Univ. Technol., Gothenburg, Sweden. 2007

[23] P. A. Jones, "Cloud-cover distributions and correlations," *J. Appl. Meteorol.*, vol. 31, pp. 732–741, Jul. 1992.

[24] H. Madsen, H. Spliid, and P. Thyregod, "Markov models in discrete and continuous time for hourly observations of cloud cover," *J. Climatol.*, vol. 24, pp. 629–639, Jul. 1985.

[25] L. B. Nielsen, L. P. Prahm, R. Berkowicz, and K. Conradsen, "Net incoming radiation estimated from hourly global radiation and/or cloud observations," *J. Climatol.*, vol. 1, no. 3, pp. 255–272, 1981.

[26] Z. Yanhui, S. Wenji, L. Shili, L. Jie, and F. Ziping, "A critical review on state of charge of batteries," *J. Renew. Sustain. Energy*, vol. 5, no. 2, p. 021403, 2013.

[27] S. Piller, M. Perrin, and A. Jossen, "Methods for state-of-charge determination and their applications," *J. Power Sour.*, vol. 96, no. 1, pp. 113–120, 2001.

[28] X. Hu, S. E. Li, and Y. Yang, "Advanced machine learning approach for lithium-ion battery state estimation in electric vehicles," *IEEE Trans. Transport. Electrific.*, vol. 2, no. 2, pp. 140–149, Jun. 2016.

[29] J. Li and W. Wei, "Probabilistic evaluation of available power of a renewable generation system consisting of wind turbines and storage batteries: A Markov chain method," *J. Renew. Sustain. Energy*, vol. 6, no. 1, p. 013139, Feb. 2014.

[30] S. X. Chen, H. B. Gooi, and M. Q. Wang, "Sizing of energy storage for microgrids," *IEEE Trans. Smart Grid*, vol. 3, no. 1, pp. 142–151, Mar. 2012.

[31] I. S. Bayram, G. Michailidis, M. Devetsikiotis, and F. Granelli, "Electric power allocation in a network of fast charging stations," *IEEE J. Sel. Areas Commun.*, vol. 31, no. 7, pp. 1235–1246, Jul. 2013.

[32] T. Robertazzi, *Computer Networks and Systems: Queueing Theory and Performance Evaluation*, 3rd ed. New York, NY, USA: Springer, 2012.

[33] A. Khodaei and M. Shahidehpour, "Microgrid-based co-optimization of generation and transmission planning in power systems," *IEEE Trans. Power Syst.*, vol. 28, no. 2, pp. 1582–1590, May 2013.

[34] C.-H. Wu, W.-C. Lee, J.-C. Ke, and T.-H. Liu, "Optimization analysis of an unreliable multi-server queue with a controllable repair policy," *Comput. Oper. Res.*, vol. 49, pp. 83–96, Sep. 2014.

[35] D. E. Goldberg, *Genetic Algorithms in Search, Optimization, and Machine Learning*. Boston, MA, USA: Addison-Wesley, Oct. 1989.

[36] T. H. Cormen, C. E. Leiserson, R. L. Rivest, and C. Stein, *Introduction to Algorithms*, 3rd ed. Cambridge, MA, USA: MIT Press, 2009, p. 799.

Juliette Ugirumurera received the B.Sc. degree in computer engineering from Oklahoma Christian University, Edmond, OK, USA, in 2012. and the M.Sc. and Ph.D. degrees in computer science from the University of Texas at Dallas, Richardson, TX, USA, in 2015 and 2017, respectively.

She is currently a Post-Doctoral Fellow with the Lawrence Berkeley National Laboratory, Berkeley, CA, USA, where she is developing high performance computing algorithms for traffic engineering problems. Her current research interests include optimization, scheduling of resources in complex networks, algorithm design, and Internet of things.

Zygmunt J. Haas (F'07) received the B.Sc. and M.Sc. degrees in electrical engineering and the Ph.D. degree from Stanford University, Stanford, CA, USA, in 1979, 1985, and 1988, respectively. He subsequently joined the Network Research Department, AT&T Bell Laboratories, where he pursued research on wireless communications, mobility management, fast protocols, optical networks, and optical switching.

From 1994 to 1995, he was with the AT&T Wireless Center of Excellence, where he investigated various aspects of wireless and mobile networking, concentrating on Transmission Control Protocol/Internet Protocol networks. In 1995, he joined the faculty of the School of Electrical and Computer Engineering at Cornell University, Ithaca, NY, USA. He joined the Computer Science Department, UT Dallas, Richardson, TX, USA, in 2013. He has authored for numerous technical papers and holds 18 patents in the fields of high-speed networking, wireless networks, and optical switching. He has organized several workshops and delivered numerous tutorials at major IEEE and Association for Computing Machinery (ACM) conferences. His current research interests include mobile and wireless communication and networks, biologically inspired networks, and modeling of complex systems.

Dr. Haas has served in the past as a Chair of the IEEE Technical Committee on Personal Communications. He is a Voting member of the ACM. He has served as an Editor of several journals and magazines, including the IEEE TRANSACTIONS ON NETWORKING, the IEEE TRANSACTIONS ON WIRELESS COMMUNICATIONS, the IEEE COMMUNICATIONS MAGAZINE, the *Springer Wireless Networks journal*, the *Elsevier Ad Hoc Networks journal*, the *Journal of High Speed Networks*, and the *Wiley Wireless Communications and Mobile Computing journal*. He has been a Guest Editor of the IEEE JOURNAL ON SELECTED AREAS OF COMMUNICATIONS issues on "gigabit networks," "mobile computing networks," and "ad-hoc networks."